Acta Cryst. (1960). **13**, 313

Twinning Caused by Abrasion on Single Crystals of Beryllium

By V. D. Scott*

Applied Physical Chemistry of Surfaces Laboratory, Chemical Engineering Department, Imperial College, London S.W. 7, England

(*Received* 24 *June* 1959 *and in revised form* 1 *September* 1959)

New results concerning the lattice re-orientation caused by abrasion on single crystals of beryllium have been obtained by electron diffraction.

The occurrence of twinning found in certain cases in sub-surface regions of abraded single-crystal beryllium surfaces was dependent upon the initial crystal orientation with relation to the direction of the applied compressive stresses. The operative $\{10\bar{1}2\}$ set of twinning planes was found to be the one which most facilitated development of the characteristic oblique [001] compression fibre texture produced by the abrasion in the outermost surface layers by rotational slip or flexural rotational slip of the sub-surface twin.

1. Introduction

Previous work on the abrasion of polycrystalline and single-crystal beryllium surfaces (Scott & Wilmaa, 1958) has shown the simultaneous occurrence of two characteristic [001] fibre orientations in the outermost surface regions. An oblique [001] fibre orientation was developed, inclined (by an angle δ) away from the outward surface normal and towards the direction from which the abrasive particles came. This main fibre orientation was shown to be a compression texture, the inclination corresponding with the angle of friction, $\tan^{-1}\mu$. The second [001] fibre orientation, with its axis normal to the surface, was associated with the amount of metal removed by shearing. In the case of an abraded beryllium single crystal, the region of transition to the underlying undisturbed beryllium lattice showed the occurrence of a heavily disoriented structure of the rotational type. It was suggested from the results that the deformation process involved flexural rotational slip on (0001), i.e. rotational slip on (0001) with simultaneous or subsequent flexure of the slip lamellae about an axis parallel to (0001) and not limited to the usual $\langle 210\rangle$ direction.

In the present work on beryllium single crystals, detailed analysis of the diffraction data indicates that in certain cases the abrasion has caused twinning of the crystal lattice. The dependence of twinning upon the crystallographic relation between the abrasion direction and the initial orientation of the single crystal is examined. The transition region from the oblique [001] fibre orientation to the twin provides further examples of flexural rotational slip.

2. Experimental details

Materials

Polycrystalline beryllium rod of 1·2 cm. diameter was machined from hot-extruded ingot produced from French Flake beryllium. The single crystals were grown from the rod by the zone-melting method.

The main impurities present in normal zone-melted material are 0·14% BeO, 0·014% Fe, 0·005% Al, 0·005% Si, 0·003% Cl, and a trace of Mg, N and F.

Preparation of specimen surfaces

After etching the beryllium single crystal in a solution of 50% aqueous H_2SO_4, fine cracks became apparent which were found to be parallel to (0001) planes.

Single-crystal faces, $(20\bar{2}3)$, $(10\bar{1}0)$, (0001) and $(10\bar{1}5)$, were prepared by cutting the crystal in the required direction (with reference to the cracks parallel to (0001)), and then smoothing the surface upon successively finer grades of emery paper down to 0000, using propyl alcohol as lubricant. The final mechanical surfacing was performed upon a rotating wheel using a diamond compound abrasive (Hyprez) of a mean particle size of 3μ. The distorted layer produced by mechanical surfacing was removed electrolytically by making the specimen anodic in a solution of 100 ml. orthophosphoric acid, 30 ml. concentrated sulphuric acid, 30 ml. ethyl alcohol and 30 ml. glycerol, as recommended by Mott & Haines (1951–2).

Abrasion experiments

The smooth specimen surfaces were abraded in a direction corresponding to a main lattice row of the Be crystal upon 000 emery paper (J. Oakey and Sons, Ltd.), using propyl alcohol as lubricant. The effect caused by abrasion on the structure of the single-crystal Be surface was investigated for an abrasion stroke length of 50 cm., at a speed of about 2 cm./s. and a load of about 1 kg. applied to the specimen.

Examination of specimen surfaces

The electron-diffraction camera was of the type described by Finch & Wilman (1937), but evacuated

* The author's present address is: The Atomic Weapons Research Establishment, Aldermaston, Berkshire, England.

by oil diffusion pumps. An accelerating potential of 50 to 60 kilovolts and a specimen-plate distance of 48 cm. were used. The orientation of the beryllium single crystals, and the structure of the deformed layer produced by the abrasion, were determined from the diffraction patterns using the methods described by Wilman (1948, 1952). They were adjusted if necessary by further abrasion and polishing to within one or two degrees of the desired orientation. Surfaces prepared in this way were relatively smooth and perfect as adjudged from the clear electron-diffraction patterns, which consisted of well-defined Kikuchi lines, usually with some spots (Figs. 1, 8 and 13). The spots were elongated normal to the shadow edge of the surface owing to refraction of the electron beam in the smooth surface of the crystal.

The specimen surfaces were examined before and after abrasion, and at various stages of removal of the surface layers by etching in 10% aqueous H_2SO_4, (which removed about 100 Å thickness per second, as estimated by weighing). Diffraction patterns were recorded at each stage, with the electron beam normal to the abrasion direction (perpendicular azimuth), parallel to it (parallel azimuth), and at chosen intermediate azimuths.

3. Experimental results

The direction of abrasion, defined as the direction of motion of the abrasive particles relative to the specimen surface, is shown by the arrows in the electron-diffraction photographs taken at the perpendicular azimuth.

(*a*) *General nature of the results*

The electron-diffraction patterns from the abraded single crystals showed in all instances the presence of an oblique [001] fibre texture and a varying proportion of normal [001] fibre texture in the upper regions of the abraded surface layer. The inclination δ, of the oblique fibre axis away from the specimen normal was within the range $21° \pm 2°$ in 20 experiments. The origin of these fibre textures and their relation to friction and wear have previously been reported, together with similar results from abraded polycrystalline Be and Mg surfaces, by Scott & Wilman (1958) and will not be discussed in detail here.

Etching away the abraded surface showed a gradual transition of the [001] axis i.e. the slip plane normal, from that of the oblique [001] fibre axis in the surface regions to that in the undisturbed single crystal, some 5μ below the surface, or to one of its twins formed during the abrasion. The azimuthal spread of orientation round the [001] axis decreased progressively (from over 30° in the outermost regions) as the undisturbed crystal was approached. In the lower region of the transition zone the main reorientation approximated to a large rotational spread (40° or more) away from the initial crystal orientation, about a relatively well-defined axis which tended to be parallel to the surface and normal to the abrasion direction. Similar examples on copper and iron have been discussed by Evans, Layton & Wilman (1951), and Agarwala & Wilman (1953, 1955).

(*b*) *Abrasion of* $(20\bar{2}3)$ *face along the* $[63\bar{4}]$ *direction (perpendicular to* [010]).

Fig. 1 shows the high perfection of the freshly-prepared crystal face as indicated by the clear Kikuchi-line and spot pattern, here obtained with the beam in the [010] direction. The (0001) slip planes were parallel to the beam and inclined at 50° to the surface, see Fig. 23.

After 5 seconds etching, exposing metal which was about 500 Å below the initial abraded surface, Fig. 2, was obtained with the beam perpendicular to the abrasion direction, and, in conjunction with the pattern obtained in the parallel azimuth, shows [001] fibre textures of the normal and inclined types with δ increased from 21° to 24°.

After a total of 10 sec. etching, the patterns (e.g. Fig. 3) showed a similar oblique fibre orientation still with more than 30° azimuthal spread round this axis as shown by the presence of a 110 diffraction arc, but with δ increased to about 40°.

After 30 sec. total etching, i.e. at 3000 Å depth, spot patterns such as Fig. 4 at the perpendicular azimuth were obtained corresponding to the initial single-crystal orientation (cf. Fig. 1). The direction of the *c*-axis, [001], which is along the row of diffraction spots of type $00l$, is inclined by 50° to the plane of incidence (i.e. the normal to the shadow edge). In addition, arcs extend from the spots clock-wise round the ring positions, with progressively decreasing intensity. This arcing, in conjunction with the symmetrical arcs (on vertical layer lines), in the pattern obtained with the beam parallel to the abrasion direction indicates a range of lattice rotations (50° or more) about the [010] direction, which was normal to the abrasion direction in the specimen surface. With further etching of the surface (up to about 5 min.) the length of the arcs was gradually reduced to zero.

(*c*) *Abrasion of* $(20\bar{2}3)$ *face along the* $\{\bar{6}\bar{3}4\}$ *direction*

The resurfaced crystal, which gave a similar diffraction pattern to Fig. 1, was abraded in the opposite direction to that in the previous experiment. The patterns from the as-abraded surface then showed the normal and inclined [001] fibre textures with $\delta = 22°$ (see § 3(*a*)).

After 20 sec. etching, the patterns (e.g. Fig. 5 at the perpendicular azimuth) showed a similar fibre orientation but with δ increased to more than 30°. The positions of the heads of the arcs in Fig. 5 correspond to the single-crystal spot pattern from the $(10\bar{1}2)$ twin, represented by the open circles in Fig. 19.

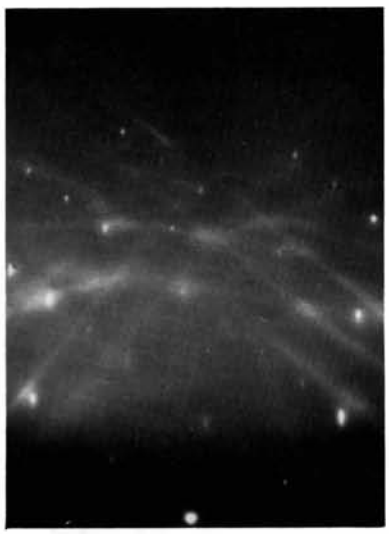

Fig. 1. Electropolished Be $(20\bar{2}3)$ face; beam [010].

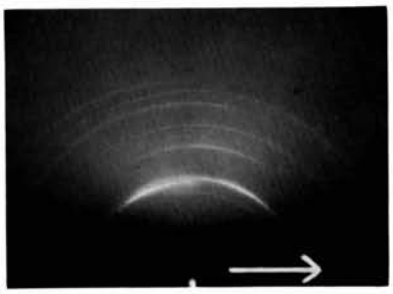

Fig. 2. As Fig. 1, abraded $[63\bar{4}]$; 5 s. etch; $\perp r$ azimuth, [010].

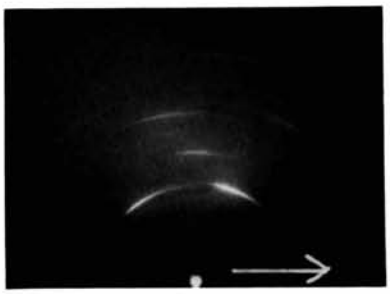

Fig. 3. As Fig. 2, 10 s. etch.

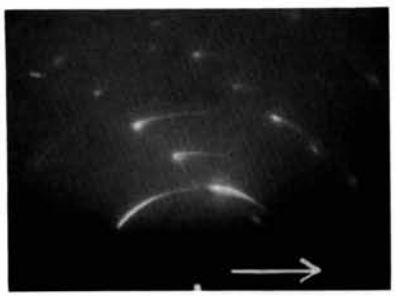

Fig. 4. As Fig. 2, 30 s. etch.

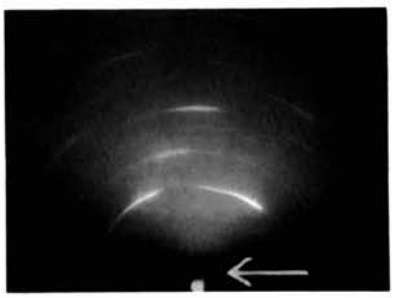

Fig. 5. As Fig. 1, abraded $[\bar{6}\bar{3}4]$; 20 s. etch; $\perp r$ azimuth, (diffractions from $(10\bar{1}2)$ twin).

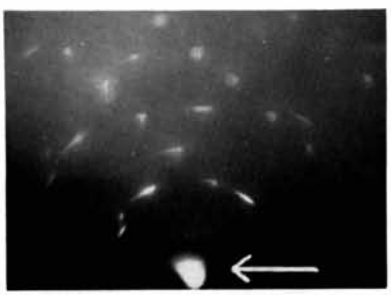

Fig. 6. As Fig. 5, 60 s. etch; (diffractions from twin and original crystal orientation).

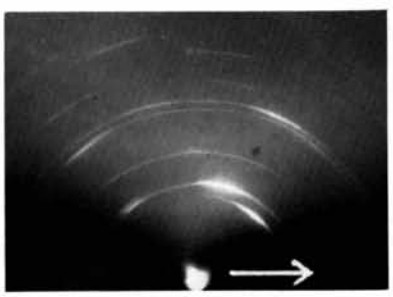

Fig. 7. Electropolished Be $(20\bar{2}3)$ face; abraded [010]; 20 s. etch; $\perp r$ azimuth.

Fig. 8. Electropolished Be (0001) face; beam [100].

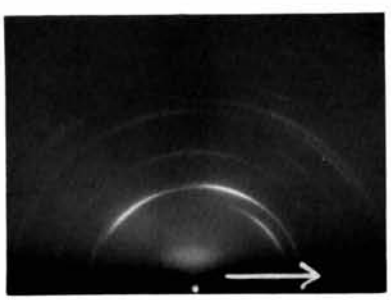

Fig. 9. As Fig. 8, abraded $[\bar{2}10]$; 5 s. etch; $\perp r$ azimuth.

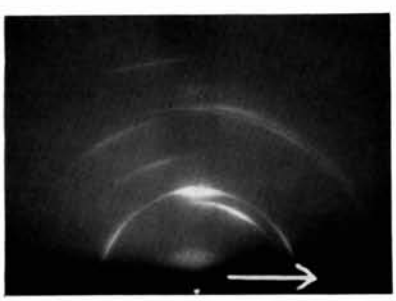

Fig. 10. As Fig. 9, 45 s. etch; $\perp r$ azimuth.

[*To face p.* 314

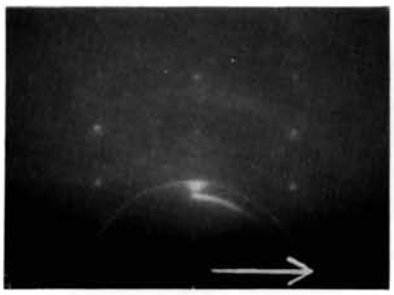

Fig. 11. As Fig. 9, 90 s. etch: (*a*) $\perp r$ azimuth.

Fig. 11. (*b*) || azimuth.

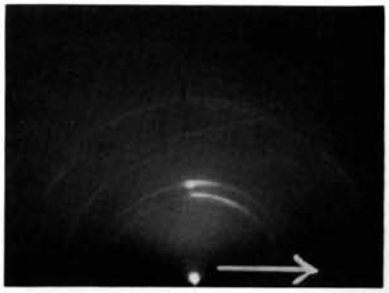

Fig. 12. As Fig. 8, abraded [$\bar{1}$00]; 90 s. etch; (*a*) $\perp r$ azimuth.

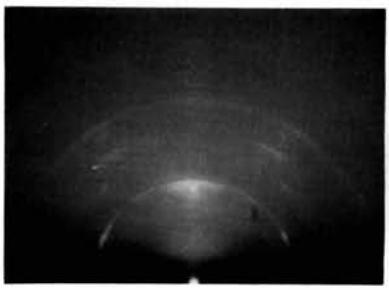

Fig. 12. (*b*) || azimuth.

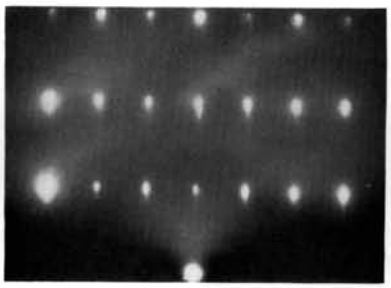

Fig. 13. Electropolished Be (10$\bar{1}$0) face: beam [100].

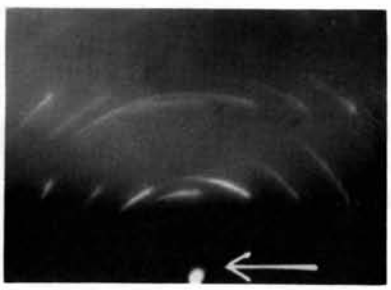

Fig. 14. As Fig. 13, abraded [001]; 30 s. etch: (*a*) $\perp r$ azimuth.

Fig. 14. (*b*) || azimuth.

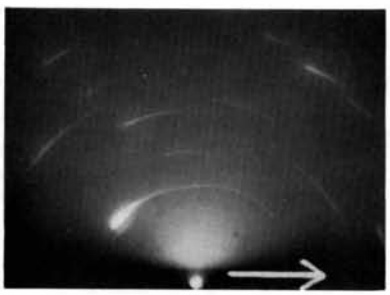

Fig. 15. As Fig. 13, abraded [010]; 120 s. etch: $\perp r$ azimuth.

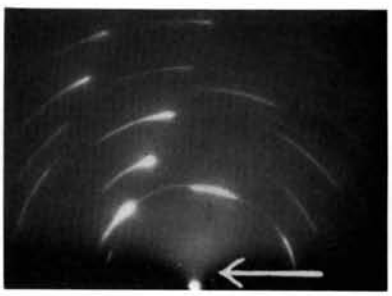

Fig. 16. Electropolished Be (10$\bar{1}$5) face; abraded [63$\bar{1}$]; 30 s. etch: $\perp r$ azimuth.

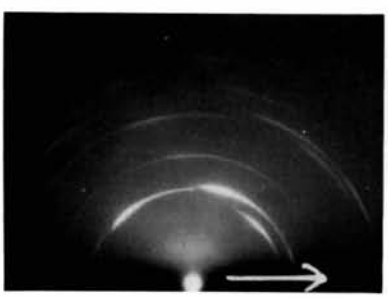

Fig. 17. Electropolished Be (10$\bar{1}$5) face; abraded [$\bar{6}\bar{3}$1]; 30 s. etch: $\perp r$ azimuth.

Fig. 18. (*a*) and (*b*). Abrasion grooves crossing a grain-boundary in polycrystalline Be.

Anti-clockwise rotation ($\sim 40°$) of this spot pattern about the beam direction, [010], i.e. the direction in the surface normal to the abrasion direction, generates the arcs seen in Fig. 5.

The relation between the initial crystal orientation and the twinned lattice is more easily seen in Fig. 6, which was obtained after 60 sec. etching (6000 Å depth below the initial surface) with the beam perpendicular to the abrasion direction. In addition to the long arcs from the rotationally disoriented twinned lattice, short arcs are now present due to the almost undistorted initial crystal lattice. This pattern shows clearly that the operative twinning plane is $(10\bar{1}2)$, i.e. the twinning plane nearly parallel to the surface.

Further etching resulted in a decrease in relative contribution to the pattern from the twin-crystal diffractions until only the pattern corresponding to the initial crystal face was obtained.

(d) Abrasion of $(20\bar{2}3)$ *face along the* [010] *direction*

The crystal was resurfaced and abraded in the [010] direction, i.e. perpendicular to the abrasion directions of § 3(*b*) and (*c*).

Fig. 7 at the perpendicular azimuth shows that after 20 sec. etching, the inclination of the [001] axis to the surface normal had increased from 21° to about 50°. This pattern is closely similar to Fig. 3(*a*). However, the orientation does not correspond to the initial crystal (since the beam direction here is at right angles to that in Fig. 3(*a*)), but to the $(1\bar{1}02)$ twin, the orientation of which is indicated in the diagram, Fig. 20. Note, for example, the *c*-axis of the twin is inclined 60° to the left of the surface normal, and that a $\langle 100 \rangle$ type of lattice row of the twin is approximately parallel to the electron beam.

The presence of additional 101, 102 and 103 arcs on the left side of the print, together with a 201 arc near the plane of incidence, indicates some twinning on another plane. This second twin-plane is clearly not $(01\bar{1}2)$, since this would result in rows of diffraction arcs similar to those observed for $(1\bar{1}02)$ twinning but with the *c*-axis inclined 60° to the right of the surface normal. The possibility of $(10\bar{1}2)$ and $(\bar{1}012)$ twinning can also be eliminated since these would produce patterns similar to Figs. 5 or 6 when viewed along the beam direction. Thus the number of possibilities is reduced to two, $(\bar{1}102)$ and $(0\bar{1}12)$ twinning. Of these, $(\bar{1}102)$ twinning accounts for the 102, 103 and 201 arcs and, possibly, the 101 arc, since some rotation of the lattice occurs about the normal to the abrasion direction in the surface. The $(\bar{1}102)$ twin is represented in Fig. 20, where the *c*-axis of the twin is seen to be inclined approximately 80° to the surface normal.

After 70 sec. etching, the pattern with the beam along [010], i.e. parallel to the abrasion direction, showed fairly long arcs corresponding to the rotation of the twinned lattice caused by the abrasion, and shorter arcs due to the initial crystal orientation.

(e) Abrasion of (0001) *face along the* $[\bar{2}10]$ *direction*

Fig. 8 was recorded from the freshly prepared surface with the beam along $\langle 100 \rangle$. After abrasion along the $[\bar{2}10]$ direction, the surface was etched for 5 sec., and the diffraction patterns (e.g. Fig. 9 at the perpendicular azimuth) showed a [001] fibre texture with δ increased from about 21° to 30°. The azimuthal spread round the [001]-axis was still more than 30°.

After 45 sec. etching, the inclination of the [001] *c*-axis to the plane of incidence had increased to 60°, Fig. 10.

Figs. 11(*a*) and (*b*), obtained after 90 sec. etching, show spots due to the initial crystal orientation, (cf. Fig. 8), and in addition, arcs due to the reorientation caused by the abrasion. These arcs indicate that twinning has occurred on either, but probably both, the $(10\bar{1}2)$ and $(\bar{1}012)$ planes. This is most clearly seen from the three symmetrical 100 arcs in Fig. 11(*b*), one in the plane of incidence and two near the shadow edge, which show that $\{10\bar{1}0\}$ planes lie approximately parallel to and at 60° to the surface, and that the [001] *c*-axis of the $(10\bar{1}2)$ and $(\bar{1}012)$ twins, (approximately parallel to the abrasion direction in the specimen surface), makes an angle of 84° and 96° respectively with the outward surface normal. The first of these two similar cases of twinning is illustrated in Fig. 21.

The length of arcing in Figs. 11(*a*) and (*b*) indicates a range of lattice rotations of approximately 40° about a [010] direction of the twinned crystal, and shows the final stages of the transition from the oblique [001] fibre texture in the outermost abraded-surface regions to the twinned crystal.

(f) Abrasion of (0001) *face along the* $[\bar{1}00]$ *direction*

The crystal was resurfaced, giving a diffraction pattern similar to Fig. 8, and then abraded in the $[\bar{1}00]$ direction.

As the surface was progressively etched, the inclination of the [001]-axis was observed to increase from about 21° until, after 90 sec. etching, Figs. 12(*a*) and (*b*) were obtained. The arcs, and in particular the 110 diffractions in 12(*b*), show twinning on the $(1\bar{1}02)$ and $(10\bar{1}2)$ planes (see Fig. 22). $\{10\bar{1}0\}$ planes of the twin lie approximately parallel to the surface in both cases, while (0001) planes of the twin are in an orientation such that they tend to be aligned more nearly normal to the abrasion direction. Sufficient spread of orientation occurs to form an almost continuous range of rotation about a [100] direction, and results in a proportion of the (0001) planes being normal to the abrasion (see three symmetrical 100 arcs in Fig. 12(*a*)). In effect this is similar to $(10\bar{1}2)$ and $(\bar{1}012)$ twinning described in § 3(*e*), although the position of 110 arcs in Fig. 12(*b*) shows that the operative twin planes are different in this case.

The length of arcing indicates a range of lattice rotations of up to 40° about a direction approximately

normal to the abrasion direction in the specimen surface, i.e. [120] of the original crystal.

(g) Abrasion of $(10\bar{1}0)$ *face along the* [001] *direction*

Fig. 13 was obtained from the freshly prepared surface with the beam along [010]. The pattern obtained after the abrasion showed that the inclination, δ, of the [001] axis of the abrasion texture was 22°.

After 30 sec. total etching, Figs. 14(*a*) and (*b*) were obtained at the perpendicular and parallel azimuths respectively. These patterns can be seen to correspond in part to the initial single-crystal orientation (cf. Fig. 13). In addition, in Fig. 14(*a*) arcs extend from the single-crystal spot positions anti-clockwise round the ring positions with progressively decreasing intensity. This arcing is similar to that described in § 3(*b*), and shows in conjunction with the positions of the symmetrical arcs in Fig. 14(*b*), a range of lattice rotations (more than 30°) about the normal to the abrasion direction in the specimen surface, i.e. [010].

(h) Abrasion of $(10\bar{1}0)$ *face along the* [010] *direction*

The resurfaced crystal gave a diffraction pattern similar to Fig. 13. The $(10\bar{1}0)$ face was then abraded along the [010] direction, i.e. parallel to (0001) slip planes.

After a total of 30 sec. etching, the inclination of the [001] axis of the fibre texture had increased from 21° at the surface to 30°. The azimuthal spread round this axis was still greater than 30°.

Fig. 15 was obtained with the beam normal to the abrasion direction after etching the surface for 120 sec., and shows an incompletely developed [001] fibre texture. The head of the strong 002 arc corresponds to an inclination of the [001] direction to the specimen normal of about 35°, indicating twinning of the lattice on $(1\bar{1}02)$ and $(\bar{1}102)$ planes, the projection of the [001] axis of the twins on the crystal surface being approximately parallel to the abrasion direction. This case is similar to the abrasion of $(20\bar{2}3)$ along [010], (cf. § 3(*d*)). Measurements of the positions of the inclined row of strong diffraction arcs in the upper right-hand corner of Fig. 15 show that they are $21l$ diffractions i.e. $(21\bar{3}0)$ planes lie perpendicular to the plane of the page and parallel to the abrasion direction. Evidently, sufficient azimuthal spread of rotation (up to 20°) is still present at this stage of etching to show $(21\bar{3}0)$ planes of the twin parallel to the abrasion direction (in addition to $(10\bar{1}0)$ planes).

(j) Abrasion of $(10\bar{1}5)$ *face along the* $[63\bar{1}]$ *direction*

The orientation of this face was adjusted such that the [001] direction of the crystal was approximately parallel to the [001] axis of the oblique fibre texture developed in the outermost surface regions, while [010] was parallel to the specimen surface (see Fig. 23).

Diffraction patterns from the freshly prepared surface were similar to Fig. 1, although the [001]-axis here was inclined 20° to the surface normal instead of 50°. After abrasion along $[63\bar{1}]$, an oblique [001] fibre texture was observed with $\delta = 20°$.

The positions of the heads of the arcs in Fig. 16, obtained at the perpendicular azimuth after 30 sec. etching, corresponds to the initial crystal orientation, while the length of arcing together with the diffraction positions in the symmetrical pattern obtained at the parallel azimuth, indicates a range of lattice rotations (20°) about [010], the normal to the abrasion direction in the specimen surface. The well-defined tail-end to the arcs in Fig. 16 shows that the amount of rotation of the (0001) planes about [010] is limited to 20°, i.e. until (0001) planes are aligned approximately parallel to the mean specimen surface; no further rotation occurs beyond this.

The very faint arcs in Fig. 16, such as 100 below the strong 002 arc near the plane of incidence, indicates a small amount of twinning. The absence of a 002 diffraction below the strong 101 arc on the left side of the print shows that $(10\bar{1}2)$ and $(\bar{1}012)$ planes are not operative, but it is not possible to identify the active twinning planes more closely than this.

(k) Abrasion of $(10\bar{1}5)$ *face along the* $[\bar{6}\bar{3}1]$ *direction*

An oblique [001] fibre orientation ($\delta = 20°$) was observed after abrading the resurfaced crystal along $[\bar{6}\bar{3}1]$, i.e. in the opposite direction to that in § 3(*j*).

Etching away the surface layers showed a progressive increase in δ until, after 30 sec. etching, Fig. 17 was obtained at the perpendicular azimuth. At this stage the azimuthal spread of orientation round the [001] axis is now less than 30°, while the [001] direction is inclined approximately 65° to the surface normal. The heads of the arcs in Fig. 17 correspond to the diffraction positions from the $(10\bar{1}2)$ twin orientation (cf. § 3(*c*)) while the length of arcing, in conjunction with the symmetrical arcs in the pattern at the parallel azimuth shows a range of lattice rotation (40°), again about [010].

With further etching, the intensity of the arcs from the twin decreased until the diffraction pattern corresponded entirely to the undisturbed, underlying crystal orientation.

4. Discussion

The occurrence of flexural rotational slip has been dealt with in an earlier paper (Scott & Wilman, 1958) but since it forms a convenient starting point for the further development of this discussion it will be briefly referred to here.

Evidence for flexural rotational slip on (0001)

The results in the cases discussed below where twinning was not observed, allow the large lattice rotations in the lower transition regions to be more

easily identified as due to flexural rotational slip on (0001) planes.

The particular example described in § 3(*b*) of a (20$\bar{2}$3) face abraded along [63$\bar{4}$] illustrates clearly the transition from the oblique [001] fibre orientation to the undisturbed single crystal. As the inclination of the [001] fibre axis changes progressively (Figs. 2 and 3), towards the value characteristic of the [001] direction of the underlying single crystal, so the extent of azimuthal spread round the fibre axis decreases. At the late stage of etching illustrated in Fig. 4, the azimuthal spread appears to be only a few degrees, while long arcs extend clockwise from diffraction spots associated with the initial crystal orientation. The disorientation then mainly consists of a wide range of rotation (~ 40°) about an axis normal to the abrasion direction and lying in or near the surface. The axis of rotation, [010], is as far away as possible (30°) in the (0001) slip plane, from the normal ⟨210⟩ flexure axis. It was suggested (Scott & Wilman, 1958) that a flexure of this observed type could be developed during or after a small extent of rotational slip on (0001) had occurred.

Thus, the deformation of the more or less fragmented surface region caused by an abrasive particle, involves near the undistorted crystal, small azimuthal rotation about [001] but large flexure, while nearer the surface the azimuthal rotation is more extensive and an oblique compression [001] fibre texture is developed.

The results from the abrasion of a (10$\bar{1}$0) face along [001], § 3(*g*) (see also a (10$\bar{1}$5) face abraded along [63$\bar{1}$], § 3(*j*)), were closely similar to the above example, again showing in sub-surface regions a wide range of lattice rotation about a ⟨100⟩ axis perpendicular to the abrasion direction in the specimen surface, explicable as due to the occurrence of flexural rotational slip on (0001).

Similar lattice rotations, about an axis which was not the normal flexure axis, were observed in the twins produced during the abrasion.

The occurrence of twinning

Twinning in beryllium occurs on (10$\bar{1}$2) planes (Mathewson & Phillips, 1928) and causes a re-orientation of the Be crystal lattice such that the (0001) slip planes are rotated about ⟨100⟩ into a position inclined 84° from the original orientation, (cf. reciprocal lattice spot pattern, Fig. 19).

Twinning occurred only in certain cases on the abraded Be single crystals. The results from six of the nine samples discussed in the present work can be conveniently represented in the diagram, Fig. 23, which shows the inclination of the [001] *c*-axis with respect to the crystal surface in these experiments. The crystal is viewed along a ⟨100⟩ type of lattice row, and the abrasion direction, i.e. the direction of motion of the abrasive particles relative to the specimen surface, is from left to right.

In two of these examples, abrasion of (20$\bar{2}$3) along [63$\bar{4}$], § 3(*b*), and abrasion of (10$\bar{1}$0) along [001], § 3(*g*), deformation by slip was observed but no twinning. Upon abrasion of the (20$\bar{2}$3) face along [$\bar{6}$3$\bar{4}$], i.e. in

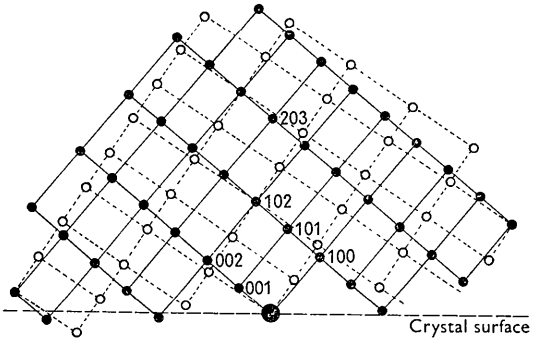

Fig. 19. Theoretical pattern from (20$\bar{2}$3) face with the beam along [010] showing also that from the twinned lattice (broken lines).

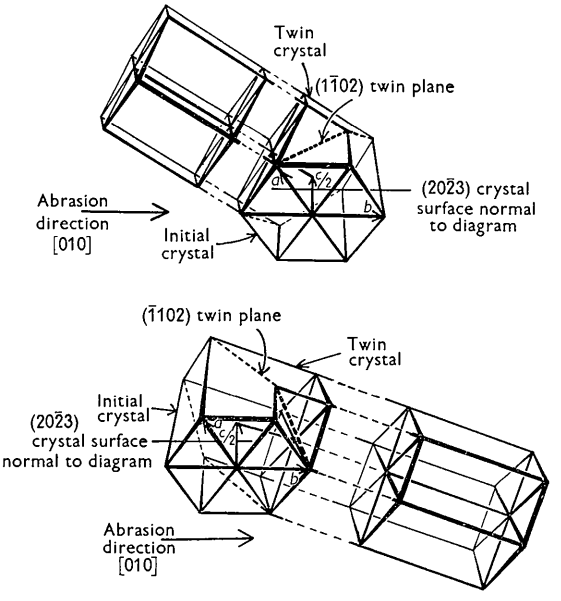

Fig. 20. Twinning on (1$\bar{1}$02) and on ($\bar{1}$102) caused by abrasion of a (20$\bar{2}$3) face along [010].

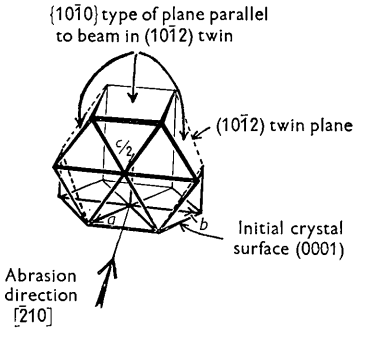

Fig. 21. Twinning on (10$\bar{1}$2) caused by abrasion of a (0001) face along [$\bar{2}$10].

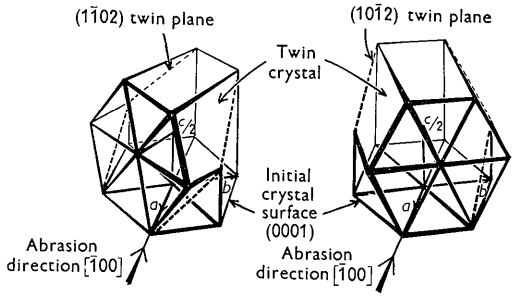

Fig. 22. Twinning on (1$\bar{1}$02) and (10$\bar{1}$2) caused by abrasion of a (0001) face along [$\bar{1}$00].

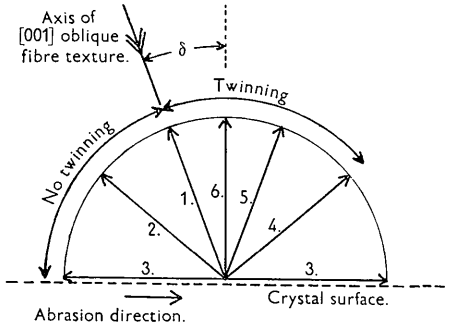

Fig. 23. The occurrence of slip and twinning with relation to the inclination of the [001] c-axis with the crystal surface and to the abrasion direction. Radial lines show [001] direction with respect to surface: [100] $\perp r$ diagram.

Example 1. (10$\bar{1}$5) surface: [63$\bar{1}$] abrasion.
Example 2. (20$\bar{2}$3) surface: [6$\bar{3}$4] abrasion.
Example 3. (10$\bar{1}$0) surface: [001] abrasion.
Example 4. (20$\bar{2}$3) surface: [$\bar{6}$34] abrasion.
Example 5. (10$\bar{1}$5) surface: [$\bar{6}$31] abrasion.
Example 6. (0001) surface: [$\bar{2}$10] abrasion.

the opposite direction to that in § 3(b), twinning was observed on (10$\bar{1}$2), the plane nearly parallel to the crystal surface, although a smaller but undetectable amount of twinning might have occurred upon other twinning planes. Similarly, (10$\bar{1}$2) twinning was observed after abrasion of (10$\bar{1}$5) along [$\bar{6}$31], § 3(k), while (10$\bar{1}$2) and ($\bar{1}$012) twinning was found after abrading the (0001) face along [$\bar{2}$10], § 3(e).

Whether or not twinning occurs appears from these results to be determined by the facility with which the oblique [001] fibre texture can be developed by rotations of the crystal lattice either from the initial crystal orientation or from a twin orientation, the sense of the lattice rotations caused by the deformation being governed by the direction of motion of the abrasive particles with relation to the crystal surface. Thus, in the case of the (0001) face abraded along [$\bar{2}$10], the oblique [001] fibre texture is not developed simply by lattice rotations in the order of 20° about [010] in the opposite sense to the abrasion nor, on the other hand, by large lattice rotations of the order of 160° in the sense of the abrasion. Instead, the lattice has twinned, the (0001) planes in the twin being inclined at 84° to the specimen surface, and the oblique [001] fibre texture is developed with rotation (~60°) of the twinned lattice in the sense of the abrasion by flexural rotational slip as described above. A similar deformation mechanism is apparent when abrading (20$\bar{2}$3) along [$\bar{6}$34], and (10$\bar{1}$5) along [$\bar{6}$31].

The (10$\bar{1}$5) face was prepared in order to study more closely the effect of abrasion upon a crystal face of such an orientation that the inclination of the basal planes to the surface was between that of the (20$\bar{2}$3) face abraded along [$\bar{6}$34], where only slip was observed, and that of the (0001) face abraded along [$\bar{2}$10], where twinning occurred. The [001] direction of this crystal was inclined at 20° to the surface normal. Thus upon abrasion along [63$\bar{1}$], the [001] c-axis was parallel to the [001] axis of the oblique fibre texture developed in the outer-most surface regions. The diffraction patterns showed that deformation took place almost entirely by slip, of the flexural-rotational type. It would appear from these results that this is the 'critical orientation' for the advent of twinning (for abrasion along a direction perpendicular to [100]). Hence, if [001] of the original crystal is inclined less than 20° to the specimen surface normal, extensive twinning is to be expected, similar to the abrasion of (0001) along [210] where [001] was normal to the surface (see Fig. 23). It is probable that the other 'critical orientation' occurs when the inclination to the surface of the (0001) planes is 90° (about [100]) from the first position.

The abrasion in the remaining three examples was along a slip direction in the (0001) plane, i.e. parallel to a ⟨100⟩ type of lattice row. Twinning occurred in all three cases, thus reorientating the lattice into a suitable position for rotations by rotational slip or flexural rotational slip and subsequent development of the [001] fibre texture. The occurrence of (1$\bar{1}$02) and ($\bar{1}$102) twinning, which was observed when abrading the (20$\bar{2}$3) face along [010], is to be expected, since then the necessary lattice rotations are only about 40°. On the other hand, reorientation from (01$\bar{1}$2) and (0$\bar{1}$12) twins is less likely in this case since it would involve more extensive lattice rotations (in the order of 100°), or secondary twinning plus further lattice rotations. Similarly, (1$\bar{1}$02) and ($\bar{1}$102) twinning can be accounted for on the (10$\bar{1}$0) face abraded along [010], and also the formation of (1$\bar{1}$02) and (10$\bar{1}$2) twins on the (0001) face abraded along [100].

Bakarian & Mathewson (1943), working on magnesium crystals, proposed that 'the operative pair of planes is the pair for which the intersection with the (0001) slip plane makes an angle as near 90° as is geometrically possible with the projection of the stress axis on the same plane.' This statement suggests that (01$\bar{1}$2) and (0$\bar{1}$12) twins should also be formed during abrasion of (10$\bar{1}$0) along [010] in addition to (1$\bar{1}$02) and ($\bar{1}$102) twins, since all four planes intersect the (0001) slip plane to make the same angle with the projection of the stress axis on this plane. However,

the present results suggest that in these abrasion experiments any selection rule for twinning planes, including that of Lee & Brick (1956) must be modified to take account of the motion of the abrasive particles on the crystal surface.

Some particularly good examples showing the dependence of deformation mechanism upon crystal orientation are illustrated in the optical micrographs, Figs. 18(*a*) and (*b*), obtained from abraded polycrystalline beryllium after removal of the uppermost surface regions by electropolishing. The appearance of the abrasion groove shows a marked change on crossing the grain boundary, and in the right hand crystal grain twin regions are developed along the groove.

To sum up, the nature of the results from all the single-crystal abrasion experiments shows that compressive forces exerted by the abrasive particles during the deformation process have caused parts of the subsurface regions of the beryllium lattice to rotate in the sense of the abrasion, so that the (0001) slip planes tend to become aligned more nearly normal to the [001] compression axis of the oblique fibre texture in the outermost surface regions, i.e. with the slip plane normal [001] more nearly parallel to the compression axis. Where the orientation of the initial crystal with relation to the direction of the stress was unfavourable for re-orientation by slip (rotational or flexural rotational) alone, the crystal lattice has twinned, whereby further slip, which before twinning would have been difficult, is made easier. (Similar phenomena have also been illustrated for zinc and cadmium crystals by Mathewson & Phillips, 1928, and Schmid & Wasserman, 1928).

The present work shows that the operative twinning plane (or planes) resulted in the twinned lattice which most facilitated the development in the twin crystal of the oblique [001] fibre texture; hence the choice was also governed by the sense of the lattice rotations, i.e. the direction of motion of the abrasive particles on the crystal surface. The active twinning planes usually led to the most effective shortening of the axis of compression, although any such general rule has to be modified to take account of the sense of the lattice rotations as determined by the motion of the abrasive particles on the crystal surface.

The author wishes to thank Mr G. C. Ellis and Dr A. J. Martin for the provision of the beryllium single crystals, and Mr W. B. H. Lord for his constant interest and encouragement. He is also indebted to Dr H. Wilman, under whose supervision the work was carried out, for helpful discussions.

The author was on detached duty from the Atomic Weapons Research Establishment, Aldermaston, during the period of this work.

References

Agarwala, R. P. & Wilman, H. (1953). *Proc. Phys. Soc.* B, **66**, 717.

Agarwala, R. P. & Wilman, H. (1955). *J. Iron Steel Inst.* **179**, 124.

Bakarian, P. W. & Mathewson, C. H. (1943). *Trans. Amer. Inst. Min.* (*Metall.*) *Engrs.* **152**, 226.

Evans, D. M., Layton, D. N. & Wilman, H. (1951). *Proc. Roy. Soc.* A, **205**, 17.

Finch, G. I. & Wilman, H. (1937). *Ergebn. exakt. Naturw.* **16**, 353.

Lee, H. T. & Brick, R. M. (1956). *Trans. Amer. Soc. Metals*, **48**, 1003.

Mathewson, C. H. & Phillips, A. J. (1928). *Amer. Inst. Min.* (*Metall.*) *Engrs.* Tech. Publ. No. 53.

Mott, B. W. & Haines, H. R. (1951–2). *J. Inst. Met.* **80**, 629.

Schmid, E. & Wasserman, G. (1928). *Z. Phys.* **48**, 370.

Scott, V. D. & Wilman, H. (1958). *Proc. Roy. Soc.* A, **247**, 353.

Wilman, H. (1948*a*). *Proc. Phys. Soc.* **60**, 341.

Wilman, H. (1948*b*). *Proc. Phys. Soc.* **60**, 416.

Wilman, H. (1952). *Acta Cryst.* **5**, 782.